Electronic and Optical Properties of Cl-doped $CH_3NH_3SnI_3$ Perovskite: A DFT Study

Abdelmounaim Laassouli[1*], *Lhouceine* Moulaoui[2], *Abdelhafid* Najim[1], *Marouane* Archi[2], *Mohamed* Karouchi[1], *Khalid* Rahmani[4], *Youssef* Lachtioui[1] and *Omar* Bajjou[1,3]

[1] Laboratory of Engineering in Chemistry and Physics of Matter (LICPM), Faculty of Sciences and Technics, Sultan Moulay Slimane University, BP 523, 23000 Beni Mellal, Morocco
[2] Research Laboratory in Physics and Sciences for Engineers (LRPSI), Poly-disciplinary Faculty, Sultan Moulay Slimane University, BP 592, 23000 Beni Mellal, Morocco
[3] UNESCO UNISA Africa Chair in Nanosciences & Nanotechnology (U2ACN2), College of Graduate Studies, University of South Africa (UNISA), Pretoria, South Africa
[4] PSES, ERC, Ecole Normale Supérieure, Mohammed V University in Rabat P. O. Box: BP5118 Takkadoum Rabat-10000, Morocco

Abstract. Organic-inorganic hybrid perovskites have emerged as promising materials for photovoltaic applications. This study investigates the impact of chlorine (Cl) doping on the electronic and optical properties of the perovskite $CH_3NH_3SnI_3$ (MA-SnI_3) using density functional theory (DFT) calculations. We explore Cl doping concentrations of 8.33%, 16.66%, and 25%, analyzing the resulting changes in bandgap, density of states, and absorption coefficient. DFT calculations reveal a significant reduction in the bandgap with increasing Cl concentration, shifting from 1.055 eV for the methylammonium tin iodide structure to 0.727 eV, 0.731 eV, and 0.792 eV for the doped structures, respectively. Analysis of the density of states highlights the influence of Cl on the electronic structure. Furthermore, the absorption coefficient increases within the visible range, suggesting enhanced light absorption capabilities. Our results are consistent with experimental observations, validating the accuracy of DFT as a tool for studying Cl-doped MA-SnI_3 perovskites and providing insights into their potential for solar cell applications.

Keywords: Perovskite, $CH_3NH_3SnI_3$, Cl-doping, DFT, TDOS, refractive index.

1 Introduction

The global pursuit of sustainable and efficient energy sources has placed perovskite materials at the forefront of materials science research, particularly in the realm of photovoltaics and energy storage. Among the diverse array of perovskite structures, hybrid organic-inorganic perovskites have emerged as revolutionary compounds for optoelectronic applications, especially in next-generation solar cells [1]. These materials offer a unique combination of exceptional optoelectronic properties, ease of fabrication, and the potential for low-cost, high-efficiency photovoltaic devices, making them a cornerstone of sustainable energy research [2]. The importance of perovskite structures extends beyond photovoltaics, as

* Abdelmounaim Laassouli : abdelmounaim.laassouli@gmail.com

evidenced by recent computational studies exploring perovskite hydrides for hydrogen storage applications [3,4]. These investigations demonstrate the versatility of perovskite-based materials in addressing various energy challenges, from solar energy conversion to clean fuel storage. The application of density functional theory (DFT) calculations in these studies highlights the power of computational methods in predicting and optimizing material properties for energy-related applications [5,6]. $CH_3NH_3SnI_3$, a tin-based hybrid perovskite, has garnered significant attention due to its remarkable light-harvesting capabilities and promising power conversion efficiencies in solar cells [7]. The exploration of tin-based perovskites is particularly crucial as they present a less toxic alternative to their lead-based counterparts, addressing environmental concerns while maintaining high performance [8]. The unique electronic structure and optical properties of $CH_3NH_3SnI_3$ make it an ideal candidate for advancing photovoltaic technology, potentially bridging the gap between laboratory efficiency and practical, large-scale deployment of perovskite solar cells. However, the path to commercialization of perovskite-based photovoltaics is hindered by challenges such as stability under operating conditions and the need for further efficiency improvements. In this context, the strategy of doping perovskite materials with different elements has emerged as a powerful approach to tailor their properties and enhance device performance [9]. Among various dopants, chlorine (Cl) has shown promise in modifying the electronic band structure and optical properties of perovskite materials, potentially addressing key limitations in stability and efficiency. The incorporation of Cl into the $CH_3NH_3SnI_3$ structure represents a critical area of investigation, with the potential to unlock significant advancements in perovskite solar cell technology. Understanding the fundamental changes induced by Cl doping at the atomic and electronic levels is essential for rational design and optimization of these materials. This approach aligns with recent computational studies on metal hydrides and perovskite hydrides, where first-principles calculations have provided valuable insights into material properties for hydrogen storage applications [10,11]. In this study, we employ density functional theory (DFT) calculations to provide a comprehensive investigation of the effects of Cl-doping on the electronic and optical properties of $CH_3NH_3SnI_3$ perovskite. By systematically analyzing the changes induced by Cl dopants in the perovskite structure, we aim to elucidate the underlying mechanisms governing the behavior of Cl-doped $CH_3NH_3SnI_3$ and its impact on photovoltaic performance. This computational approach allows us to probe atomic-level interactions and electronic structure modifications that are challenging to observe experimentally, providing valuable insights for materials design and optimization.

Our research not only advances the fundamental understanding of Cl-doped $CH_3NH_3SnI_3$ perovskite but also offers practical guidance for the design and optimization of novel perovskite-based solar cells with enhanced efficiency and stability. By clarifying the complex interplay between dopants, electronic structure, and optical properties, this work contributes to the ongoing efforts to overcome current limitations in perovskite photovoltaics. The insights gained from this study have broad implications for the field of sustainable energy technologies, potentially accelerating the development of high-performance, environmentally friendly solar cells that can meet the growing global demand for clean energy. Moreover, the computational methodologies employed in this study align with recent trends in materials science research, where DFT calculations have been successfully applied to investigate a wide range of energy-related materials, from photovoltaics to energy storage systems. This broader context underscores the significance of our work in contributing to the computational toolset for designing and optimizing materials across various energy applications, fostering a more comprehensive approach to addressing global energy challenges.

2 Computational Methods

Electronic and optical properties of $CH_3NH_3SnI_3$ perovskite were investigated using DFT calculations implemented in the Cambridge Sequential Total Energy Package (CASTEP) [12]. The Perdew-Burke-Ernzerhof (PBE) functional within the generalized gradient approximation (GGA) was employed [13]. Ultrasoft pseudopotentials were used to represent the interactions between core and valence electrons, with on-the-fly generated (OTFG) pseudopotentials describing electron-ion interactions [14]. A plane-wave energy cutoff of 550 eV was used for all calculations. The Brillouin zone was sampled using a 2×4×2 k-point grid. The Pulay density mixing method was adopted for self-consistent field operations, with a convergence criterion of 10^{-5} eV/atom [15]. Maximum stress was set to 0.05 GPa [16]. Valence electron configurations were as follows: C: $2s^2 2p^2$, H: $1s^1$, N: $2s^2 2p^3$, Sn: $5s^2 5p^2$, I: $5s^2 5p^5$, and Cl: $3s^2 3p^5$.

The geometry of the $CH_3NH_3SnI_3$ structure was optimized before calculating electronic and optical properties. A supercell of cubic $CH_3NH_3SnI_3$ structure in the alpha phase with P4mm symmetry with lattice parameters $a = b = c = 6.23$ Å and $\alpha = \beta = \gamma = 90°$ was studied. Different Cl doping concentrations were investigated by systematically replacing specific I atoms with Cl atoms in the supercell.

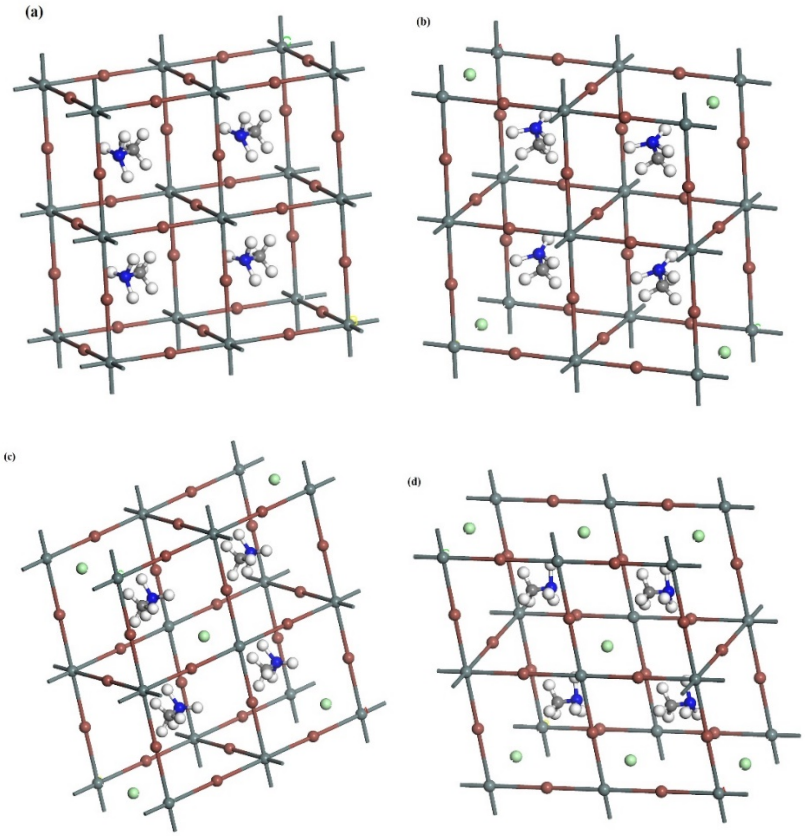

Fig. 1. Crystal structure of $CH_3NH_3SnI_3$ (a), $CH_3NH_3SnCl_{0.02}I_{2.98}$ (b), $CH_3NH_3SnCl_{0.04}I_{2.96}$ (c), and $CH_3NH_3SnCl_{0.06}I_{2.94}$ (d).

3 Results and Discussions

3.1 Electronic Properties

3.1.1 Band Gap

The electronic band structures of methylammonium tin iodide and chlorine-doped $CH_3NH_3SnI_3$ perovskite materials, illustrated in Figure 2, reveal critical insights into their electronic properties. The four panels depict energy bands along high-symmetry points in the Brillouin zone (G-F-Q-Z-G), with energy expressed in electron volts (eV) [17]. A systematic modulation of the band gap (Eg) is observed, ranging from 1.055 eV [18] for the $CH_3NH_3SnI_3$ material to 0.727 eV, 0.731 eV, and 0.792 eV for the Cl-doped samples, respectively. It's noteworthy that the observed band gap value for this material is comparatively smaller than the band gaps of $MAGeI_3$ and $MASnI_2Br$ which stand at 1.54 eV and 1.70 eV respectively[19,20]. The band gap (Eg) is determined by calculating the energy difference between the valence band maximum (VBM) and the conduction band minimum (CBM) at the same k-point in the Brillouin zone. For a direct band gap material, as observed in this case, both the VBM and CBM are located at the same k-point, specifically at the F point. The calculation of Eg involves first identifying the highest occupied energy level, corresponding to the VBM, at the F point. Then, the lowest unoccupied energy level, representing the CBM, is identified at the same point. The energy gap is obtained by subtracting the energy of the VBM from that of the CBM, yielding $Eg = E_{CBM} - E_{VBM}$. These direct band gaps, manifesting at the F point, suggest favorable optoelectronic characteristics [21].

The band structures consistently exhibit direct gaps across all compositions, with the conduction band minimum and valence band maximum coinciding at the F point. This feature is maintained throughout the doping series, indicating that Cl incorporation modulates the band gap magnitude without fundamentally altering the electronic structure. The observed dispersion characteristics of the valence and conduction bands remain qualitatively similar across the series, further supporting this interpretation. Panel (b) displays the $CH_3NH_3SnI_3$ with its 1.055 eV band gap, while panels (a), (c), and (d) showcase the Cl-doped variants with their progressively altered band gaps. The systematic reduction in band gap energy with Cl doping suggests a potential mechanism for fine-tuning the material's optoelectronic properties. This tailorability is particularly relevant for optimizing performance in photovoltaic and optoelectronic applications. The comparative analysis of these band structures elucidates the impact of Cl doping on the electronic properties of $CH_3NH_3SnI_3$ perovskite. The observed narrowing of the band gap with Cl incorporation may enhance light absorption capabilities, a crucial factor for improving the efficiency of photovoltaic devices. Moreover, the preservation of the direct gap nature across the doping series suggests that the

favorable optical transition of the methylammonium tin iodide material is likely maintained in the doped variants.

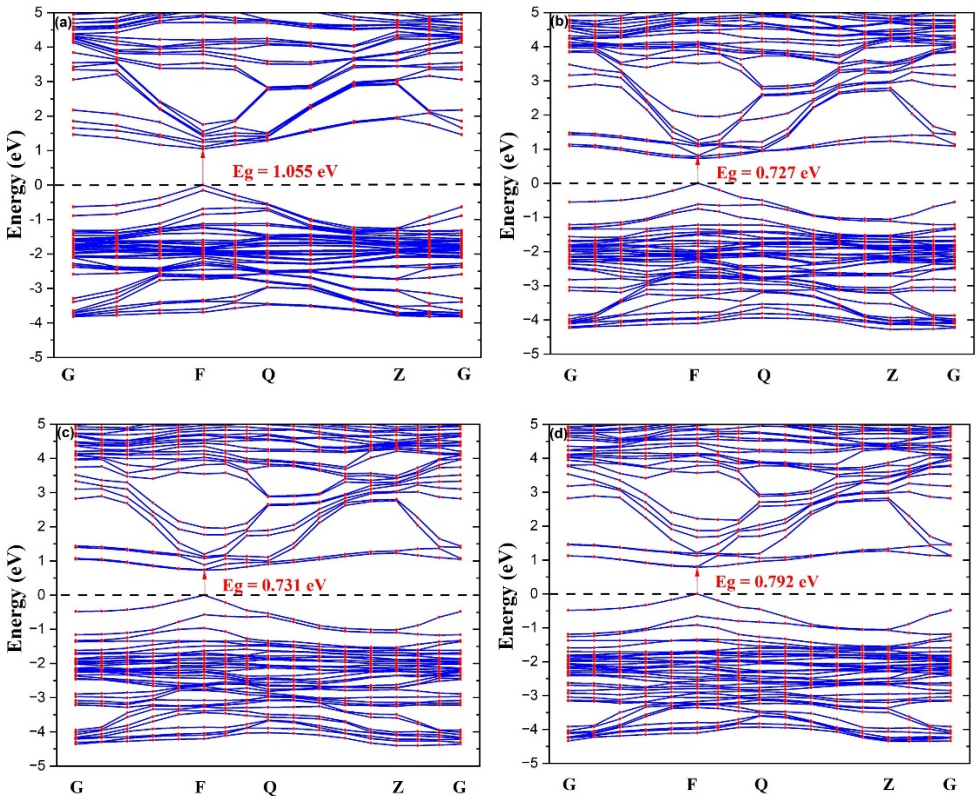

Fig. 2. Band structures of of $CH_3NH_3SnI_3$ (a), $CH_3NH_3SnCl_{0.02}I_{2.98}$ (b), $CH_3NH_3SnCl_{0.04}I_{2.96}$ (c), and $CH_3NH_3SnCl_{0.06}I_{2.94}$ (d).

3.1.2 Total Density of States

The total density of states (TDOS) profiles offers valuable insights into the electronic structure of the investigated tin-based perovskite materials. Across all compositions, the TDOS exhibits consistent overall features, characterized by prominent peaks in the valence band region and a more continuous distribution in the conduction band [22]. The introduction of chlorine dopants induces subtle yet significant alterations in the TDOS, particularly near the band edges [23]. Figure 3 presents a comparative analysis of the TDOS for $CH_3NH_3SnI_3$ and its chlorine-doped variants ($CH_3NH_3SnCl_{0.02}I_{2.98}$, $CH_3NH_3SnCl_{0.04}I_{2.96}$, and $CH_3NH_3SnCl_{0.06}I_{2.94}$). The TDOS is plotted as a function of energy, with the Fermi level (Ef) set at 0 eV. While the valence band region (negative energies) displays similar features across all compositions, including prominent peaks around -2 eV and -6 eV, the introduction of chlorine dopants leads to notable changes in the TDOS profile. $CH_3NH_3SnI_3$ exhibits a relatively smooth conduction band, whereas the Cl-doped samples demonstrate more pronounced peaks and structural features in this region, particularly between 2-6 eV. Moreover, the overall intensity of the TDOS increases with Cl doping, especially in the conduction band, indicating an enhancement in available electronic states. This effect is most pronounced for the highest doping concentration ($CH_3NH_3SnCl_{0.06}I_{2.94}$).

Interestingly, the bandgap appears to remain relatively consistent across all compositions, as evidenced by the similar onset of states near the Fermi level. The highest occupied states show subtle variations in peak intensities and positions as the chlorine content increases, which may influence the optoelectronic properties of these materials [24]. These observations suggest that chlorine doping modifies the electronic structure of $CH_3NH_3SnI_3$, potentially enhancing its optoelectronic properties by increasing the density of available states for charge carriers. This could have significant implications for charge transport and recombination processes in perovskite-based devices.

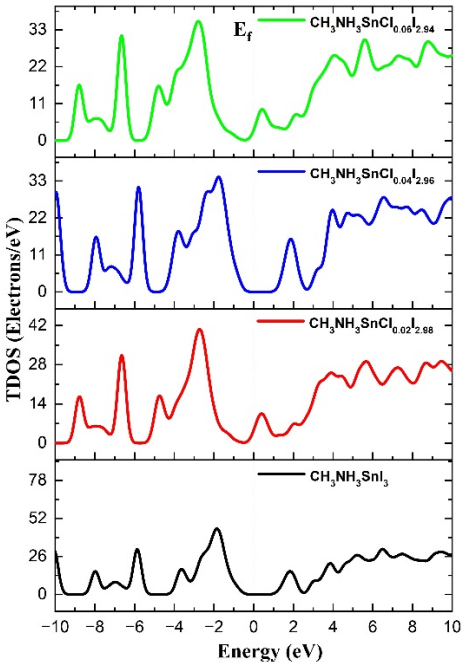

Fig. 3. TDOS of $CH_3NH_3SnI_3$, $CH_3NH_3SnCl_{0.02}I_{2.98}$, $CH_3NH_3SnCl_{0.04}I_{2.96}$, and $CH_3NH_3SnCl_{0.06}I_{2.94}$.

3.2 Optical Properties

3.2.1 Absorption Coefficient

Light absorption in a medium involves the transfer of photon energy to matter via electron interactions. The absorption coefficient, a key parameter in this process, quantifies the penetration depth of light at specific wavelengths before absorption occurs [25]. This metric plays a critical role in understanding and optimizing the conversion efficiency of solar energy systems. The description of material absorption can be articulated using the following formula:

$$\alpha(\omega) = 2\omega \sqrt{\frac{-\varepsilon_1(\omega)}{2} + \sqrt{\frac{(\varepsilon_1(\omega))^2 + (\varepsilon_2(\omega))^2}{2}}} \quad (1)$$

Figure 4 illustrates the calculated absorption coefficients of $CH_3NH_3SnI_3$ and its chlorine-doped derivatives ($CH_3NH_3SnCl_{0.02}I_{2.98}$, $CH_3NH_3SnCl_{0.04}I_{2.96}$, and $CH_3NH_3SnCl_{0.06}I_{2.94}$) as a function of wavelength. The spectra reveal significant modifications in the optical properties

upon chlorine incorporation. All compositions exhibit intense absorption in the ultraviolet region, characterized by a prominent peak at approximately 75 nm. However, the most notable alterations occur in the visible and near-infrared regions. The undoped $CH_3NH_3SnI_3$ displays a broad absorption band centered around 300 nm, which shifts to approximately 350 nm and shows enhanced intensity in the Cl-doped variants. This red shift and amplification of absorption suggest improved light-harvesting capabilities across the visible spectrum for the doped samples. Notably, the Cl-doped structures demonstrate consistently higher absorption coefficients in the 400-700 nm range compared to their methylammonium tin iodide counterpart, potentially translating to enhanced photovoltaic performance. Interestingly, the magnitude of Cl doping (ranging from 0.02 to 0.06) appears to exert minimal influence on the overall absorption profile, indicating that even modest halide substitution can induce substantial alterations in the material's optical properties.

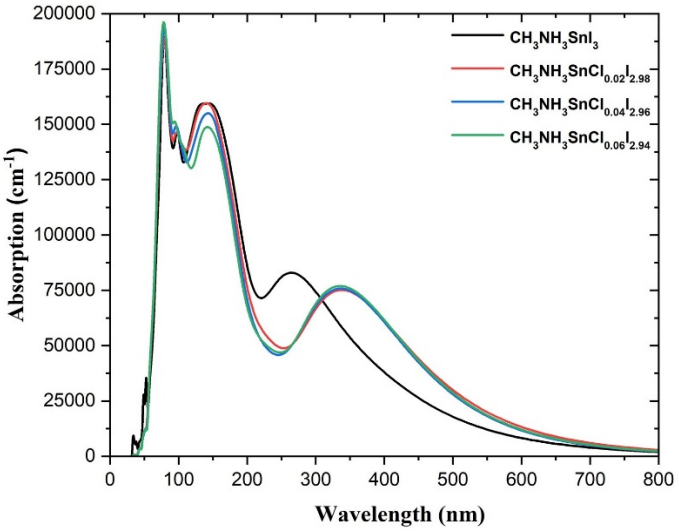

Fig. 4. Calculated absorption coefficients of pure $CH_3NH_3SnI_3$ and doped structures $CH_3NH_3SnCl_xI_{3-x}$ (x = 0.02, 0.04, 0.06) as a function of wavelength.

3.2.2 Dielectric Function

The dielectric function, a crucial parameter describing the interaction of light with matter, provides a powerful framework for understanding and predicting the optical and electronic properties of crystalline solids [26]. This function, denoted as $\varepsilon(\omega)$, is a complex quantity that encapsulates the material's response to an applied electric field as a function of the frequency (ω) of the incident light. It can be expressed as:

$$\varepsilon(\omega) = \varepsilon_1(\omega) + i\varepsilon_2(\omega) \quad (2)$$

where $\varepsilon_1(\omega)$ and $\varepsilon_2(\omega)$ are the real and imaginary parts of the dielectric function, respectively. The Kramers-Kronig relations can be used to derive the real component of the dielectric function from its imaginary part. The imaginary part of the dielectric function is particularly important for calculating the optical constants of materials. The dielectric function was calculated for both pure and Cl-doped $CH_3NH_3SnI_3$. In the real part of the dielectric function (Figure 6a), all compositions show a strong initial increase in the dielectric constant up to around 300 nm, followed by a peak in the 300-400 nm range. The undoped $CH_3NH_3SnI_3$ displays a maximum value near 6, while chlorine doping results in a slight elevation of this peak, indicating enhanced dielectric response due to Cl incorporation. The

variations among the different doping levels (0.02, 0.04, 0.06) are minimal, suggesting that even low levels of chlorine doping can effectively modify the material's dielectric properties. For the imaginary part of the dielectric function (Figure 6b), which correlates with the material's absorption characteristics, a similar trend is observed. The $CH_3NH_3SnI_3$ shows a pronounced peak around 400 nm, which shifts to higher wavelengths and increases in magnitude upon chlorine doping. This indicates an enhanced absorption capability in the visible range for the Cl-doped samples, which aligns with improved photovoltaic performance. Notably, the highest absorption is observed for the $CH_3NH_3SnCl_{0.02}I_{2.98}$ composition, with a gradual decrease in intensity for higher doping levels, suggesting an optimal doping concentration for maximizing absorption.

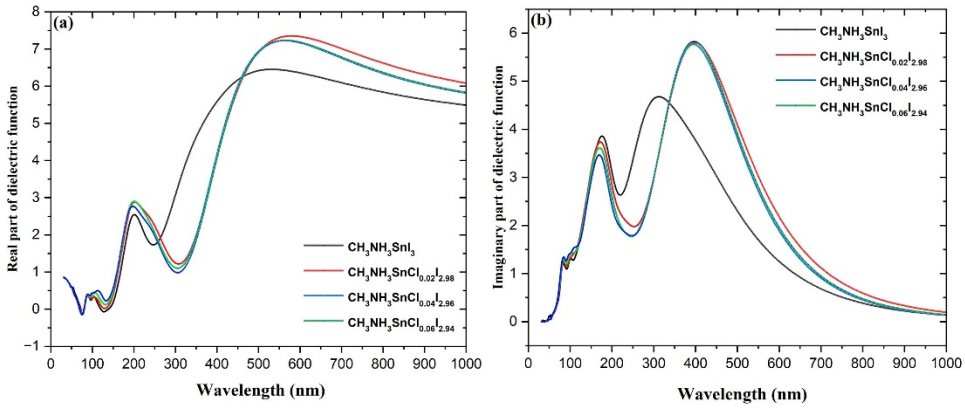

Fig. 6. Real (a) and imaginary (b) parts of the dielectric function of $CH_3NH_3SnI_3$, doped $CH_3NH_3SnI_3$ perovskite with Cl

3.2.3 Refractive Index

The refractive index, which quantifies how light propagates through a medium, was calculated for both pristine and Cl-doped $CH_3NH_3SnI_3$. In the context of optical properties, the refractive index is expressed as a complex function [27].

$$n^*(\omega) = n(\omega) + ik(\omega) \tag{3}$$

where ω represents the angular frequency of light. This complex representation delineates the refractive behavior, characterized by the real part n(ω), from the light absorption, described by the imaginary part k(ω), also known as the extinction coefficient [28].

$$n(\omega) = \sqrt{\frac{\varepsilon_1(\omega)}{2} + \sqrt{\frac{(\varepsilon_1(\omega))^2 + (\varepsilon_2(\omega))^2}{2}}} \tag{4}$$

$$k(\omega) = \sqrt{\frac{-\varepsilon_1(\omega)}{2} + \sqrt{\frac{(\varepsilon_1(\omega))^2 + (\varepsilon_2(\omega))^2}{2}}} \tag{5}$$

In the refractive index plot (Figure 7a), the undoped $CH_3NH_3SnI_3$ shows a sharp increase in the refractive index in the UV region, peaking around 1.5 at approximately 250 nm. Chlorine doping leads to an increase in the refractive index, particularly in the visible to near-infrared regions (400-800 nm), where the Cl-doped samples exhibit higher refractive indices compared to the $CH_3NH_3SnI_3$ material. This indicates that Cl doping enhances the optical

density of the material, which could be beneficial for applications requiring high refractive index materials.

The extinction coefficient (Figure 7b), which measures the material's absorption loss, shows similar trends. The undoped $CH_3NH_3SnI_3$ has a peak around 350 nm, which shifts to higher wavelengths and increases in magnitude upon chlorine doping. This suggests that chlorine incorporation not only shifts the absorption edge but also enhances the material's overall absorption capacity. The Cl-doped samples show higher extinction coefficients across the visible spectrum, with the most pronounced effect observed for the $CH_3NH_3SnCl_{0.02}I_{2.98}$ composition. Overall, the refractive index and extinction coefficient analyses reveal that chlorine doping significantly modifies the optical properties of $CH_3NH_3SnI_3$. The enhanced refractive index and extinction coefficient in the Cl-doped samples suggest improved optical performance, making these materials more suitable for photovoltaic and optoelectronic applications.

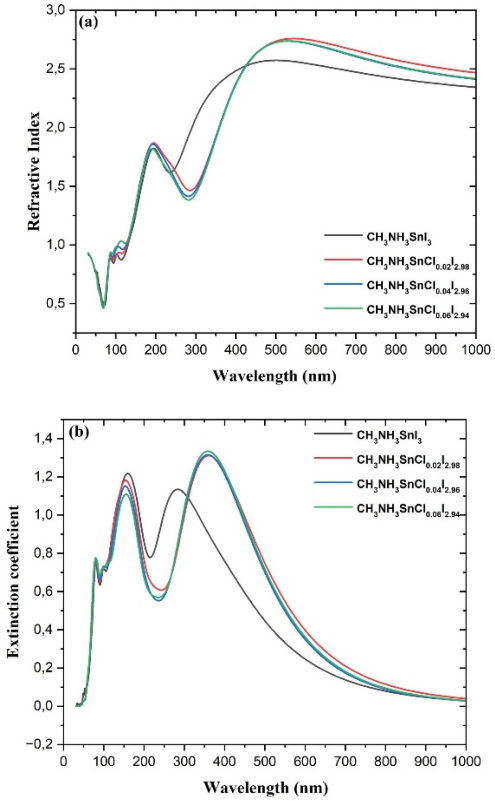

Fig. 7. Refractive index (a) and extinction coefficient (b) of $CH_3NH_3SnI_3$, doped $CH_3NH_3SnI_3$ perovskite with Cl.

4 Conclusion

This study elucidates the influence of Cl doping on the electronic and optical properties of $CH_3NH_3SnI_3$ perovskites using DFT calculations. Our results reveal that Cl doping

significantly reduces the bandgap, which shifts from 1.055 eV in the methylammonium tin iodide structure to values as low as 0.727 eV for the doped structures. This reduction in bandgap enhances light absorption capabilities, particularly in the visible range. The TDOS analysis indicates that Cl incorporation modifies the electronic structure by increasing the density of available states for charge carriers, particularly in the conduction band. This alteration is expected to enhance charge transport and reduce recombination losses in solar cell devices. Furthermore, the optical properties of Cl-doped $CH_3NH_3SnI_3$ exhibit enhanced absorption coefficients and dielectric functions in the visible spectrum. This improvement suggests that Cl-doped $CH_3NH_3SnI_3$ perovskites can effectively harvest more sunlight, leading to better performance in photovoltaic applications. The increased refractive index and extinction coefficient in the doped samples further support the material's suitability for optoelectronic devices.

References

1. A. Kojima, K. Teshima, Y. Shirai, and T. Miyasaka, J Am Chem Soc 131, 6050 (2009)
2. L. Moulaoui, O. Bajjou, A. Najim, K. Rahmani, A. Marouane, A. Laassouli, Y. Lachtioui, and B. Manaut, in 2023 3rd International Conference on Innovative Research in Applied Science, Engineering and Technology (IRASET) (IEEE, 2023), pp. 1–7
3. Benaali, H., Bahhar, S., Tahiri, A., Didi, Y., Fatihi, H., Abbassi, A & Naji, M. (2024). Investigation of KMnH3 and KFeH3 perovskite hydrides via ab-initio for hydrogen storage. Inorganic Chemistry Communications, 113033.
4. Didi, Y., Bahhar, S., Tahiri, A., Naji, M., & Rjeb, A. (2024). A Computational Study of Metal Hydrides Based on Rubidium for Developing Solid-State Hydrogen Storage. ChemistrySelect, 9(22), e202401444.
5. Bahhar, S., Tahiri, A., Jabar, A., Louzazni, M., Idiri, M., & Bioud, H. (2024). Computational assessment of MgXH3 (X= Al, Sc and Zr) hydrides materials for hydrogen storage applications. International Journal of Hydrogen Energy, 58, 259-267.
6. Bahhar, S., Jabar, A., Tahiri, A., Moubah, R., Idiri, M., & Bioud, H. (2024). X2CoH5 (X= Ca, Sr) for hydrogen storage: First-principles computations. International Journal of Hydrogen Energy, 83, 1320-1330.
7. F. Hao, C. C. Stoumpos, D. H. Cao, R. P. H. Chang, and M. G. Kanatzidis, Nat Photonics 8, 489 (2014)
8. M. Archi, O. Bajjou, L. Moulaoui, A. Najim, M. Karouchi, K. Rahmani, and B. El haddadi, in 2023 3rd International Conference on Innovative Research in Applied Science, Engineering and Technology (IRASET) (IEEE, 2023), pp. 1–7
9. N. K. Tailor, M. Abdi-Jalebi, V. Gupta, H. Hu, M. I. Dar, G. Li, and S. Satapathi, J Mater Chem A Mater 8, 21356 (2020)
10. Benaali, H., Bahhar, S., Fatihi, H., Tahiri, A., Naji, M., Abbassi, A., & Manaut, B. (2024, May). First-Principles Screening of Structural, Electronic and Elastic Properties of Sr-Based Hydrides-Perovskites Sr XH 3 (X= Ti, M n and Fe) for Hydrogen Storage Applications. In 2024 4th International Conference on Innovative Research in Applied Science, Engineering and Technology (IRASET) (pp. 01-05). IEEE.
11. Bahhar, S., Tahiri, A., Jabar, A., Louzazni, M., Idiri, M., & Bioud, H. (2024). DFT-based first-principles calculations of new NaXH3 (X= Ti, Cu) hydride compounds for hydrogen storage applications. Computational Materials Science, 238, 112928.

12. M. Karouchi, O. Bajjou, H. Jabraoui, A. Ejjabli, M. Archi, L. Moulaoui, K. Rahmani, and Y. Lachtioui, in 2023 3rd International Conference on Innovative Research in Applied Science, Engineering and Technology (IRASET) (IEEE, 2023), pp. 1–7
13. A. Najim, O. Bajjou, A. Bakour, and K. Rahmani, J Electron Spectros Relat Phenomena 265, 147321 (2023)
14. L. Moulaoui, O. Bajjou, A. Najim, and K. Rahmani, E3S Web of Conferences 336, 000 15 (2022)
15. L. Moulaoui, A. Najim, A. Laassouli, M. Archi, A. Bakour, Y. Lachtioui, K. Rahmani, O. Bajjou, and B. Manaut, E3S Web of Conferences 469, 00086 (2023)
16. A. Najim, O. Bajjou, A. Bakour, M. Boulghallat, and K. Rahmani, Modern Physics Letters B 38, (2024)
17. A. Laassouli, O. Bajjou, Y. Lachtioui, A. Najim, L. Moulaoui, and K. Rahmani, in 2023 3rd International Conference on Innovative Research in Applied Science, Engineering and Technology (IRASET) (IEEE, 2023), pp. 1–6
18. R. Sabetvand, M. E. Ghazi, and M. Izadifard, J Comput Electron 19, 70 (2020)
19. Y. Jiao, Y. Lv, J. Li, M. Niu, and Z. Yang, Comput Theor Chem 1114, 20 (2017)
20. F. J. Berger, I. Poli, E. Aktas, S. Martani, D. Meggiolaro, L. Gregori, M. D. Albaqami, A. Abate, F. De Angelis, and A. Petrozza, Supporting Information for How Halides Alloying Influences the Optoelectronic Quality in Tin-Halide Perovskite Solar Absorbers (n.d.)
21. C. Paschal, A. Pogrebnoi, T. Pogrebnaya, and N. Seriani, SN Appl Sci 2, 718 (2020)
22. A. Najim, O. Bajjou, M. Boulghallat, M. Khenfouch, K. Rahmani, and Y. Chrafih, Optik (Stuttg) 257, 168874 (2022)
23. A. Najim, O. Bajjou, M. Boulghallat, K. Rahmani, and L. Moulaoui, E3S Web of Conferences 336, 00006 (2022)
24. M. Archi, M. Al-hattab, O. Bajjou, L. Moulaoui, K. Rahmani, and B. Elhadadi, Journal of Nanoparticle Research 26, 138 (2024)
25. Y. Zhang, C.-K. Lim, Z. Dai, G. Yu, J. W. Haus, H. Zhang, and P. N. Prasad, Phys Rep 795, 1 (2019)
26. A. Najim, O. Bajjou, L. Moulaoui, A. Laassouli, M. Archi, A. Bakour, Y. Lachtioui, and K. Rahmani, in 2023 3rd International Conference on Innovative Research in Applied Science, Engineering and Technology (IRASET) (IEEE, 2023), pp. 1–5
27. G. Nazir, A. Ahmad, M. F. Khan, and S. Tariq, Computational Condensed Matter 4, 32 (2015)
28. H. Lashgari, A. Boochani, A. Shekaari, S. Solaymani, E. Sartipi, and R. T. Mendi, Appl Surf Sci 369, 76 (2016)